A R C H I V E S O F M E T A L L U R G Y A N D M A T E R I A L S
Volume 53 2008 Issue 4

Y. EICHHAMMER* **, J. ROECK*, N. MOELANS*, F. IACOPI**, B. BLANPAIN*, M. HEYNS**

CALCULATION OF THE Au-Ge PHASE DIAGRAM FOR NANOPARTICLES

OBLICZENIE WYKRESU FAZOWEGO Au-Ge W SKALI NANO

The CALPHAD (CALculation of PHAse Diagrams) method provides a powerful tool for the calculation of phase diagrams. It is based on thermodynamic databases gathering information on the relative stabilities of pure substances and mixing properties of alloys. We have added a size dependent contribution to an existing CALPHAD description of the Au-Ge bulk system. The parameters are optimized using composition and temperature dependent surface energies calculated according to the Butler model. The effect of particle size on the phase diagram is discussed for spherical nano-particles.

Metoda CALPHAD jest doskonałym narzędziem do obliczania wykresów fazowych na podstawie danych termodynamicznych gromadzonych w różnych bazach danych. W pracy niniejszej dodano czynnik uwzględniający wielkość ziaren materiału do istniejącego opisu temodynamicznego układu Au-Ge. Parametry termodynamiczne zoptymalizowano stosując zależne od składu i temperatury energie powierzchniowe, wyliczone modelem Butlera. Rozpatrzono efekt wpływu rozmiaru cząstek na topologię wykresu fazowego zakładając kulisty kształt cząsteczek.

1. Introduction

Systems in the 1-100nm show unique features, due to so-called size effects. These effects influence for example the melting temperature [1], solubility [2] and the electronic [3] and magnetic [4] properties of a system under study. Consequently, an important effort is carried out in the scientific community to understand these materials and to be able to produce them in a reproducible manner. Large scale application [5] will then be possible. Primarily, these effects can be understood by the fact that the ratio of surface to volume atoms is much higher for nanomaterials than for their bulk counterparts. Thus, their influence on the properties of the system under study can not be neglected. In this study we are interested in the changes in thermodynamic properties and phase equilibria a system undergoes when decreasing its size, such as a decrease in melting point for pure elements or a depression of the liquidus line in the case of alloys.

The CALPHAD (CALculation of PHAse Diagrams) method [6] provides a powerful tool for the calculation of phase diagrams based on thermodynamic Gibbs free energy expressions for pure substances and the mixing properties of solutions. This method combines thermodynamic modeling with experimental data. The models are phenomenological. Experimental data are required to determine the parameters in the model using an optimization procedure.

Purpose of this work was to extend the classical CALPHAD-approach for bulk materials to the calculation of phase diagrams for nano-systems. Our calculations rely on the use of existing thermodynamic databases, developed in the framework of the CALPHAD community. A corrective term taking surface effects into account is added to the Gibbs energy expressions previously determined for bulk systems. The parameters in this corrective term must be assessed based on surface properties, such as surface tension, of the alloys. In this paper, the binary Au-Ge system will be taken as an example, due to its possible applications in nanocrystal growth [7].

One must be aware that the proposed classical thermodynamic approach is only valid if the number of atoms is large enough to ensure statistic relevance of the calculations. It can however be shown that classi-

* DEPARTMENT OF METALLURGY AND MATERIALS ENGINEERING, KATHOLIEKE UNIVERSITEIT LEUVEN, KASTEELPARK ARENBERG 44, 3001-HEVERLEE, BELGIUM
** IMEC, KAPELDREEF 75, 3001-HEVERLEE, BELGIUM

cal thermodynamics remains relevant for nanoparticles having a radius larger than ~2nm [8].

2. Thermodynamic equations

We will derive the equations assuming a binary system A-B. The total Gibbs free energy of a nanosystem can be written as:

$$G^{system} = G^{bulk} + G^{surface} \quad (1)$$

with G^{bulk} and $G^{surface}$ being the bulk and surface part of the Gibbs free energy of the system, expressed in J/mol. According to standard thermodynamics for solutions [6], the molar Gibbs free energy of the bulk is expressed as:

$$G^{bulk} = X_A G_A^0 + X_B G_B^0 + RT(X_A \ln X_A + X_B \ln X_B) + G^{ex,bulk} \quad (2)$$

with X_A and X_B the atomic fraction of components A and B, G_A^0 and G_B^0 the standard Gibbs free energies of A and B, R the universal gas constant, T the temperature and $G^{ex,bulk}$ the excess Gibbs free energy of the system. In the CALPHAD approach, the excess Gibbs free energy is usually modeled with a Redlich-Kister expansion, which yields [6]:

$$G^{ex,bulk} = X_A X_B \Sigma L^j (X_A - X_B)^j. \quad (3)$$

The interaction parameters Lj are expressed as functions of temperature:

$$L^j = a + bT + cT\ln T + \ldots \quad (4)$$

For spherical and isotropic particles, the molar surface Gibbs free energy can be expressed using a Gibbs-Thomson formula:

$$G^{surface} = 2C\sigma V/r, \quad (5)$$

where σ is the surface tension of the alloy, V the molar volume of the alloy and r the radius of the particle. C is a correction factor that is often introduced to take the effect of shape and elasticity into account [9] (C=1 and1.05 for liquids and solids respectively).

The molar volume V is expressed as a linear combination of the molar volumes of the pure elements :

$$V = XAVA + XBVB, \quad (6)$$

which means that we neglect volume effects.

For nanoparticles a size dependence must be added to the standard Gibbs free energy (equations (2)). If a spherical particle of the pure element and the same size is chosen as the reference state, it follows from equation (5) that

$$G_i^{0,nano} = G_i^0 + 2C\sigma_i V_i/r \quad (7)$$

with G_i^0 the standard reference energy of the corresponding bulk phase. Consequently we can rewrite the Gibbs free energy of a nano system in the following way:

$$G^{system} = X_A G_A{}^{0,nano} + X_B G_B{}^{0,nano} + RT(X_A \ln X_A + X_B \ln X_B) + G^{ex,nano}. \quad (8)$$

By combining equations (1) and (8) one obtains:

$$G^{ex,nano} = G_{system} - X_A G_A{}^{0,nano} - X_B G_B{}^{0,nano} - RT\,(X_A \ln X_A + X_B \ln X_B). \quad (9)$$

As for bulk materials, $G^{ex,nano}$ is modeled with a Redlich-Kister expansion, but a size dependence is introduced in the expression of the interaction parameters. Thus:

$$G^{ex,nano} = X_A X_B E_i^{Lj,nano} (X_A - X_B)^j, \quad (10)$$

with

$$L^{j,nano} = a + a1/r + (b + b1/r)T + (c + c1/r)T\ln T + . \quad (11)$$

A simple inverse dependence with respect to the radius of the nanoparticle is assumed for the interaction parameters.

The parameters a, b, ... in equation (11) are the same as those in equation (4) for the bulk phase. Combining equations (9),(10) and (11) yields:

$$a1 + b1T + c1T\ln T + \cdots = 2C(\sigma_{alloy} V_{alloy} - X_A \sigma_A V_A - X_B \sigma_B V_B) \quad (12)$$

This provides an appropriate expression for the assessment of the coefficients a1,a2, ... in the interaction parameters, which are consequently determined in a phenomenological manner. Surface tension data are required to optimize these coefficients.

3. Calculation of surface tension for alloys

Since experimental data on surface energies of alloys are scarce, the surface tension of the liquid phase is calculated with the Butler equation [10]:

$$\begin{aligned}\sigma_{alloy} &= \sigma_A + (RT/A_A)\ln(X_A^{surface}/X_A^{bulk}) + (1/A_A)(G_A^{ex,surface}(T, X_A^{surface}) - G_A^{ex,bulk}(T, X_A^{bulk})) \\ &= \sigma_B + (RT/A_B)\ln(X_B^{surface}/X_B^{bulk}) + (1/A_B)(G_B^{ex,surface}(T, X_B^{surface}) - G_B^{ex,bulk}(T, X_B^{bulk}))\end{aligned} \quad (13)$$

where A_i is the molar surface of pure element A or B. $G_i^{ex,surface}$ is the partial excess Gibbs free energy of the surface of element i. It can be linked to the partial bulk excess free energy of the surface [11] as

$$G_i^{ex,surface} = \beta G_i^{ex,bulk}, \quad (14)$$

β is estimated to be 0.85 for liquids and 0.84 for solids [9].

Molar surface can be linked to molar volume in the following way:

$$A_i = 1.091 N_A^{1/3} V_i^{2/3}, \quad (15)$$

where N_A is Avogadro's number.

Butler's equation is solved by an iterative method (Newton-Raphson method in this case), giving the surface composition and surface tension of an alloy A-B.

In the case of solids, Butler's equation can be used as well if the effects of shape and surface strain are not too important,

These composition and temperature dependent surface energies are used to determine the parameters a1, b1, ... in the interaction parameters (12).

4. Assessment of the parameters

The method developed above allows us to assess Gibbs free energy expressions for nano systems. Expressions of the form (12) for the interaction parameters are then used as an input in conventional thermodynamic databases, which can in turn be used in the usual software using these databases (Thermocalc, Pandat, FactSage,...).

The lattice stabilities of the pure elements were reassessed using equation (7) and the interaction parameters using equation (12). All parameters for the bulk contribution in the Gibbs free energy are taken from the SSOL4 database [12]. Physical properties used in the calculation are listed in Table 1.

TABLE 1

Physical properties used in the calculations

Surface tension

Solid

$\sigma_S^{Ge} = 1.32$ J/m2 [9]
$\sigma_S^{Au} = 1.947 - 0.43*10 - 3T$ J/m2 [17]

Liquid

$\sigma_l^{Au} = 1.33 - 1.4*10\text{^}(-4)*T$ [9]
$\sigma_l^{Ge} = 0.941 - 2.6*10\text{^}(-4)*T$ [18]

Molar Volumes

Solid

$V_{m,s}^{Au} = 1.015e\text{-}05$ m3/mol
$V_{m,s}^{Ge} = 1.36e-05 m3/mol$

Liquid

$V_{m,l}^{Au} = 1.02582*10\text{^}(-5)+7.797*10\text{^}(-10)*T$ J/m2 [9]
$V_{m,l}^{Ge} = 1.465*10\text{^}(-5)+1.175*10\text{^}(-9)*T$ J/m2 [18]

Thermodynamic parameters used for the reassessment of the system are listed in Table 2. The corrective terms determined in this work are added as well.

TABLE 2

Size dependent lattice stabilities and interaction parameters

The bulk contributions are taken from [12], the size dependent contributions have been obtained in this work.

Gold

Liquid phase

298.15<T<929.4

$G^{o,liq}_{Au}$-$G^{o,fcc}_{Au}$ = 5613.144+97.444232*T-22.75455*T*LN(T)-
0.00385924*T^2+3.79625*10^(-7)*T^3-25097*T^(-1)+2.464*10^(-5)/r-1.906*10^(-9)*T/r+5.18*10^(-13)*T^2/r

929.4<T<1337.33

$G^{o,liq}_{Au}$-$G^{0,fcc}_{Au}$ = - 81034.481 + 1012.30956*T-155.706745*T*LN(T)+.08756015*T^2-1.1518713*10^(-5)*T^3+10637310*T^(-1) +
2.464*10^(-5)/r-1.906*10^(-9)^{8}T/r+5.18*10^(-13)*T^2/r

1337.33<T<1735.8

$G^{o,liq}_{Au}$-$G^{o,fcc}_{Au}$ = 326619.829-2025.76412*T+263.252259*T*LN(T)-0.118216828*T^3-67999832*T^(-1) +2.464*10^(-5)/r-1.906*10^(-9)
*T/r+5.18*10^(-13)*T^2/r

1735.8<T<3200

$G^{o,liq}_{Au}$-$G^{o,fcc}_{Au}$ = 418.217 + 155.886658*T-30.9616*T*LN(T) +2.464*10^(-5)/r-1.906*10^(-9)*T/r+5.18*10^(-13)*T^2/r

Fcc phase

298.15<T<929.4

$G^{o,fcc}_{Au}$ = -6938.856+ 106.830098*T-22.75455*T*LN(T)-0.00385924*T2+3.79625*10^(-7)*T^3-25097*T^(-1)+3.310*10^(-5)/r

929.4<T<1337.33

$G^{o,fcc}_{Au}$ = 93586.481 + 1021.69543*T-155.706745*T*LN(T)+0.08756015*T^2-1.1518713*10$^{|wedge}$3+10637210*T^(-1) +3.310*10^(-5)/r

1337.33<T<1735.8

$G^{o,fcc}_{Au}$ = 314067.829-2016.37825*T + 263.252259*T*LN(T)-0.118216828*T^2+8.923844*10^(-6)*T^3-67999832*T^(-1) + 3.310*10^(-5)/r

1735.8<T<3200

$G^{o,fcc}_{Au}$ = -12133.783+165.272524*T-30.9616*T*T*LN(T) + 3.310*10^(-5)/r

Germanium

Liquid phase

298.15<T<900

$G^{o,liq}_{Ge}$-$G^{o,dia}_{Ge}$ = 27655.337 + 134.94853*T-29.5337682*T*LN(T)+0.005568297*T^2-1.513694*10^(-6)*T^3 + 163298*T^(-1)+8.56632*10^(-21)
*T^7+2.02*10*(-5)/r 3.92*10^(-9)*T/r-6.11 * 10^(-13)*t^2/r

900<T<1211.4

$G^{o,liq}_{Ge}$-$G^{o,dia}_{Ge}$ = 31452.25+72.173826*T-19.8536239*T*LN(T)-0.003672527*T^2+8.56632*10^(-21)*T^7+2.02*10^(-5)/r-3.92*10^(-9)*
T/r-6.11*10^(-13)*T^2/r

1211.4<T<3200

$G^{o,liq}_{Ge}$-$G^{o,dia}_{Ge}$ = 27243.473+126.324186*T-27.6144*T*LN(T) + 2.02*10^(-5)/r-3.92*10^(-9)*T/r-6.11*10^(-13)*T^2/r

Diamond phase

298.15<T<900

$G^{o,dia}_{Ge}$ = -9486.153+165.635573*T-29.5337682*T*LN(T)+0.005568297*T**2-1.513694E-06*T**(-1)+3.26E-05/r

900<T<1211.4

$G^{o,dia}_{Ge}$ = -5689.239+102.86087*T-19.8536239*T*LN(T)-0.003672527*T2+3.26E-05/r

1211.4<T<3200

$G^{o,dia}_{Ge}$ = -9548.204 + 156.708024*T-27.6144*T*LN(T)-8.59809*10^(28)*T^(-9) + 3.26E-05/r

Fcc phase

298.15<T<900

$G_{Ge}^{o,fcc}-G_{Ge}^{o,dia}$ = + 26513.847 + 143.335573*T-29.5337682*T*LN(T)+0.005568297*T^2-1.513694*10^(-6)*T^3+ 163298*T^(-1) + 3.26e-05/r

900<T<1211.4

$G_{Ge}^{o,fcc}-G_{Ge}^{o,dia}$ = + 30310.761 + 80.56087*T-19.8536239*T*LN(T)-0.003672527*T^2+3.26E-05/r

1211.4<T<3200

$G_{Ge}^{o,fcc}-G_{Ge}^{0,dia}$ = + 26451.796+134.408024*T-27.6144*T*LN(T)-8.59809*10^(28)*T^(-9) +3.26E-05/r

Interaction parameters

Liquid phase

L^0 = - 18059.75-13.08541*T-3.0402*10^(-5)/r+1.9768*10^(-7)*T/r-5.9115*10^(-10)*T^(2)/r+7.9129*10^(-13)*T^(3)/r-4.8975*10^(-16)*T^(4)/r+ 1.410*10^(-19)*T^(5)/r

$L1$ = - 6131.6-9.10177*T-15234*10^(-5)/r+7.6301*10^(-8)*T/t-2.4785*10^(-10)*T^(2)/r + 3.5839*10∧(-13)*T^(3)r-2.3317*10^(-16)*T^(4)/r+ 5.6068*10^(-30)*T^(5)r

L2 = - 4733.85-3.25908*T-1.5669* 10^(-6)/r-3.4062* 10^(-8)*T/r+6.9529*10^(-11)*T^(2)/r-5.1279*10^(-14)*T^(3)/r+1.3084*10^(-17)*T^(4)/r

L^3 = - 8120.5-5.82538*T

Fcc phase

L^0 = 14369.4-28.58012*T-4.5605*10^(-5)/r+3.1624*10^(-7)*T/r-9.3365*10^(-10)*T^(2)/r+1.2484*10^(-12)*T^(3)/r-7.7067*10^(-16)*T^(4)/r+ 1.7908*10^(-19)*T^(5)/r

These values were used to create a thermodynamic database, which was in turn used with the Thermocalc software to calculated phase diagrams.

5. Phase diagram

Calculated phase diagrams for different system sizes are shown in Fig 1. We can observe a liquidus depression as the system size is decreased. The eutectic temperature is also lowered, and we can also observe a shift in eutectic composition.

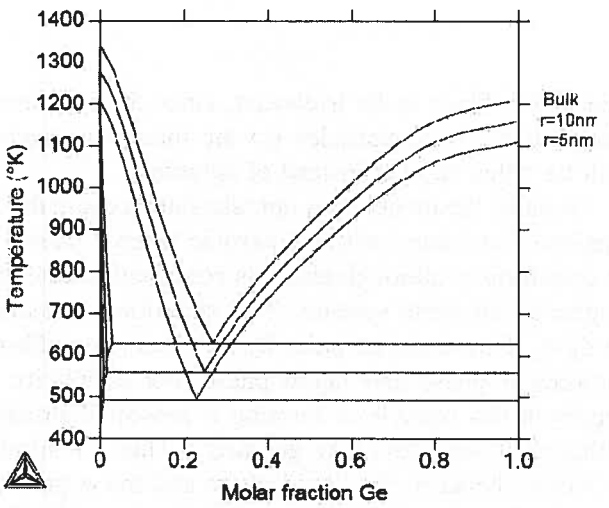

Fig. 1. Au-Ge phase diagram for nano particles with radius r=5nm and r=10nm along with the bulk phase diagram for comparison

In Fig 2a, a zoom of the Au rich region is shown. We can observe that for a given temperature the solubility of Ge in the fcc phase is increased when decreasing the size of the system. If we zoom on the Ge-rich side of the phase diagram (Fig 2b), we do not observe such an increase in solid solubility. The reason for this is however that the diamond phase is modeled without solubility of Au. In order to check whether there is an increase of the solubility with decreasing particle size, a lattice stability for Au in the (bulk) diamond phase and an interaction parameter for Au-Ge are required. These are however not available and difficult to estimate.

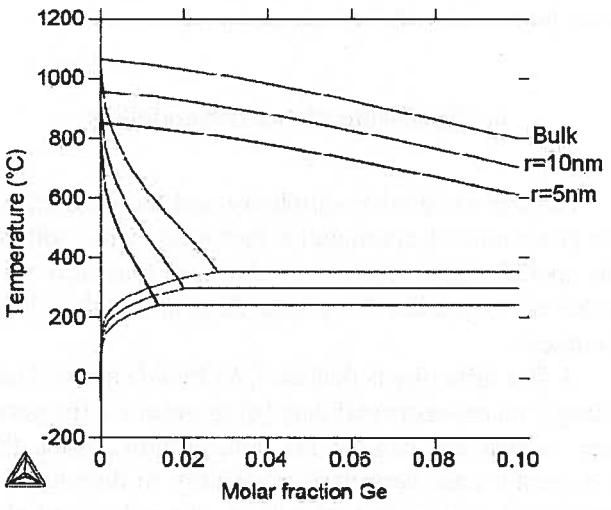

Fig. 2a. Zoom on the Au rich region of the phase diagram

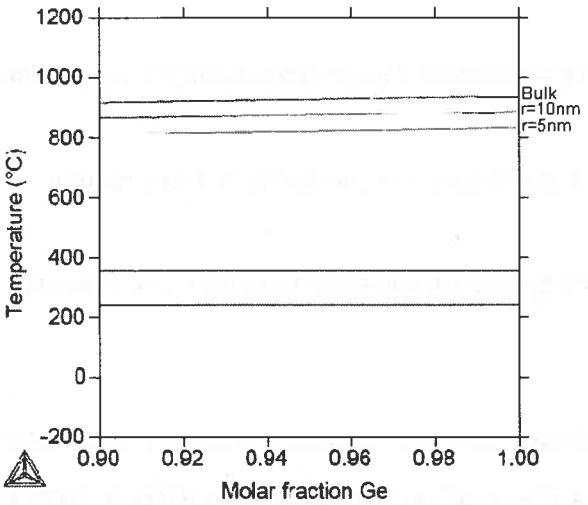

Fig. 2b. Zoom on the Ge rich region of the phase diagram

The decrease in melting temperatures [13], depression of the liquidus line [14] and increase in solid solubility are expected [2] (agree with experimental observation). The melting point depression of Au is compared to the experiment of Buffat et al.[15], and shows a good agreement (fig. 3). Unfortunately, no experimental data is available for other regions of the phase diagram to our knowledge.

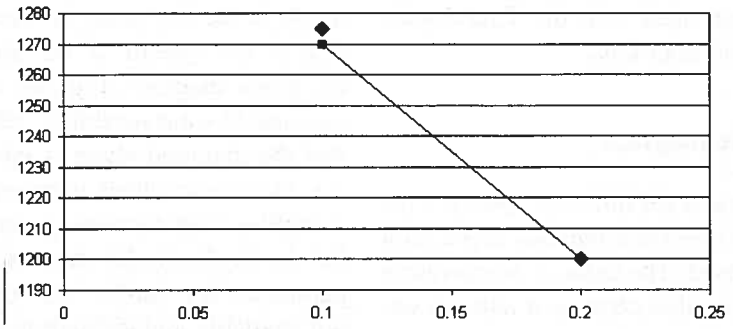

Fig. 3. Comparison of the calculated melting point of Au with experimental values of Buffat and Borel [15]. The line is for calculated values and the diamonds for experimental values

6. Discussion of the methodology

Despite its relative simplicity and the possibility to use conventional commercial thermodynamic software, this model shows certain weaknesses that have to be corrected to predict the phase diagrams with a higher accuracy.

A first difficulty is that the CALPHAD method relies strongly on experimental data [6] to optimize the parameters, which are lacking for nanosystems. Thus, there is currently only very little possibility to determine the parameters accurately and validate the calculated phase diagrams.

Secondly, the description of the surface properties of solids is dramatically simplified in this model. Especially for highly anisotropic materials, like germanium, expression (5) is likely to be irrelevant, since the equilibrium shape of the nano particles (in the diamond structure) will be rather faceted instead of spherical.

Finally, the model does not take into account the formation of interfaces within a particle when 2 phases are in equilibrium, although also this contribution cannot be neglected for small systems. This situation is illustrated in fig 4. If we consider point B, we observe equilibrium between α phase and liquid phase. For simplicity, we represent this particle as forming a core-shell structure, although it may have any geometry. Thus an interface is formed between the liquid phase and the α phase. In the classical thermodynamic software, the state of the coexisting phases would be characterized by drawing a common tangent to the two energy curves for a given temperature. Points A and C would then yield the

equilibrium compositions of the coexisting phases. This approach is however no longer possible if the interface energy between both phases has to be taken into account. A more suitable method is described by Jesser et al [16] and will be applied in further work.

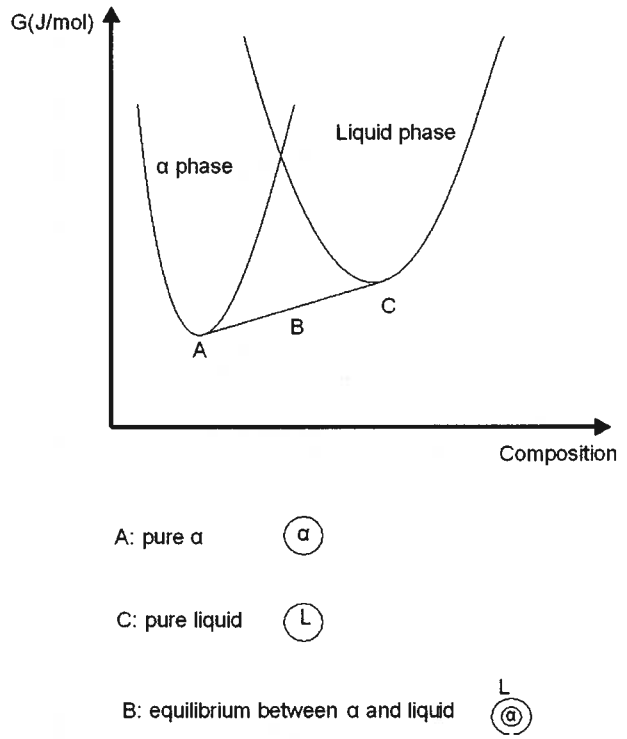

Fig. 4. Illustration of the common tangent construction and its shortcomings. Situation A is pure α, situation C pure liquid and situation B equilibrium between the two phases

7. Conclusions

An assessment of the Au-Ge nanosystem has been carried out in this paper. An existing thermodynamic description of the bulk system developed in the framework of the CALPHAD approach was adapted to take surface energy into account. The calculated phase diagrams are qualitatively in good agreement with experimental observations. They predict for example a decrease of the melting temperature with decreasing particle size, which is also found experimentally. However, further studies using a more realistic description of the nanosystem under consideration, must be performed to obtain accurate quantitative results. Experimental data on surface tension, surface segregation and particle shape are also of crucial importance to improve the exixting models for nano systems.

Received: 20 September 2008.

REFERENCES

[1] M. Wautelet, Appl. Phys. **24**, 343-346 (1991).
[2] 2: J.-G. Lee, H. Mori, Eur. Phys. J. D **34**, 227-230 (2005).
[3] J.-A. Yan, L. Yang, M. Y. Chou, Phys. Rev. B **76**, 115319 (2007).
[4] H. Naganuma, K. Sato, Y. Hirotsu, J. Magn. Magn. Mater. **310**, 2356-2358 (2007).
[5] A. S. Verhulst, W. G. Vandenberghe, K. Maex, G. Groeseneken, Appl. Phys. Lett. **910**, 53102 (2007).
[6] N. Saunders, A. P. Miodownik, CALPHAD : a comprehensive guide (1998, 0-08-042129-6 , Pergamon).
[7] S. Kodambaka, J. Tersoff, MC Reuter and FM Ross, Science **316**, 729-732 (2007).
[8] M. Wautelet, D. Duvivier, Eur. J. Phys. **28**, 953-959 (2007).
[9] J. Park, J. Lee, CALPHAD **32**, 135-141 (2008).
[10] J. A. V. Butler, P ROY SOC A-MATH PHY **135**, 348 (1932).
[11] T. Tanaka, K. Hack, T. Iida, S. Hara, Z. Metallkd. **87**, 380-389 (1996).
[12] SSOL4 database.
[13] M. Zhang, M. Y. Efremov, F. Schietekatte, E. A. Olson, A. T. Kwan, S. L. Lai, T. Wisleder, J. E. Green, L. H. Allen, Phys. Rev. B **62**, 10548 (2000).
[14] H. D. Park, A. C. Gaillot, S. M. Prokes, R. C. Cammarata, J. Cryst. Growth **296**, 159-164 (2006).
[15] P. Buffat, J.-P. Borel, Phys. Rev. A **13**, 2287-2298 (1976).
[16] W. A. Jesser, R. Z. Schneck, W. W. Gile, Phys. Rev. B **69**, 144121 (2004).
[17] A. A. Stekolnikov, F. Bechstedt, Phys. Rev. B **72**, 125326 (2005).
[18] Iida et al., The physical properties of liquid metals (1993, 0-19-856394-9 ,Oxford)